Research Square

Preprints are preliminary reports that have not undergone peer review.
They should not be considered conclusive, used to inform clinical practice,
or referenced by the media as validated information.

Displacement-Induced OFF-ON-OFF Detection of Aluminum and Cyanide in Water: Environmental Monitoring, Bioimaging, and In Vitro/In Vivo Analysis

Kemal Yararli
Bingöl University
Abdullah Saleh Hussein
Salahaddin University-Erbil
Funda Keteci
Atatürk University
Ozge Turbedaroglu
Atatürk University
Buket Bakan
Atatürk University
Turgay Sisman
Atatürk University
Ozkan aksakal
Atatürk University
Sinan Bayindir
sbayindir@bingol.edu.tr
Bingöl University
Ferruh Lafzi
Atatürk University

Research Article

Keywords: Rhodamine, Aluminum, Cyanide, Living Cells Imaging, RGB-analysis, Daphnia magna

Posted Date: June 1st, 2026

DOI: https://doi.org/10.21203/rs.3.rs-9721650/v1

License: This work is licensed under a Creative Commons Attribution 4.0 International License.
Read Full License

Additional Declarations: No competing interests reported.

Version of Record: A version of this preprint was published at Microchimica Acta on July 1st, 2026. See the published version at https://doi.org/10.1007/s00604-026-08250-w.

Abstract

In this work, a new probe called **Rh-Ph-Rh** that features two rhodamine groups attached to a phenyl ring was developed. This hybrid compound serves multiple purposes: it turns on with a strong fluorescent signal in the presence of aluminum ions (Al^{3+}) and can detect them at concentrations as low as 358 nM. Interestingly, when both Al^{3+} and cyanide ions (CN^-) are present, fluorescence is quenched, enabling sensitive detection of CN^- (*down to 619 nM*). Beyond sensing, **Rh-Ph-Rh** can act as a molecular "memory" unit and displays notable electrical properties. Moreover, practical applications include the rapid detection of Al^{3+} and CN^- ions using filter paper strips and smartphone-based RGB colorimetric analysis. In biological assays using MCF-7 cancer cells, **Rh-Ph-Rh** exhibited anticancer effects that increased with higher doses (IC_{50} = 31.357 μg/mL), enabling fluorescence-based imaging of aluminum ions within cells. Tests in live *Daphnia magna* (water fleas) confirmed that a visible green glow could selectively identify Al^{3+}. Taken together, these results suggest that **Rh-Ph-Rh** could be a valuable tool for environmental monitoring, biological imaging, and cancer treatment and diagnosis.

1. Introduction

Recently, there's been a noticeable shift toward the use of organic-based materials in sensor technology [1–4]. In ion detection, simple methods such as colorimetry and fluorometry are becoming increasingly popular, primarily because they offer sensitive, affordable alternatives to traditional analytical techniques [5–7]. This trend highlights the need for selective detection of ions in complex mixtures using organic compounds [8–11]. Among these, rhodamine derivatives have become a staple in the design of fluorescent sensors, owing to their high brightness, photostability, and broad emission range. Of these, rhodamine stands out for its remarkable photophysical qualities. Rhodamine is particularly valued in fields such as live-cell imaging and ion detection, owing to its strong light absorption and high quantum yield [12]. One of its unique features is reversible switching between non-fluorescent and fluorescent forms, making it ideal for creating highly selective and sensitive sensors [13]. However, rhodamine is not without its drawbacks. Its relatively bulky structure and hydrophobic nature can reduce its solubility and make it harder for cells to take up [14]. There is also the risk of high background fluorescence or non-specific interactions, which can sometimes lead to misleading, false-positive results. Nonetheless, despite these challenges, rhodamine continues to play a key role in the development of advanced, sensitive, and selective sensor technologies, thereby maintaining its position at the forefront of research in this area [15, 16]. This research focuses on detecting aluminum ions, achieving sensitivity levels that meet international detection standards. Aluminum (Al^{3+}), which is abundant in Earth's crust, is a corrosion-resistant and lightweight metal. Therefore, it can be used in many industrial parts, such as in airplanes, cars, food packaging, and building materials [17, 18]. Although beneficial, overexposure to aluminum can be harmful, making it a hazardous waste that must be monitored in natural resources and biological processes. Research conducted in recent years shows that aluminum can cause neurological problems, including issues with the kidneys, respiratory system, bones, and Alzheimer's disease [19–21]. Therefore, to protect human and environmental health and reduce these risks, organizations like the

World Health Organization (WHO) recommend keeping daily aluminum intake between 3 and 10 mg. This limit is set at 5 mg/L (7.41 μM) in drinking water [22–24]. Similarly, cyanide is extremely toxic and can be lethal even at very low levels, which is why drinking water standards are so strict, typically around 1–2 μM. For example, the WHO recommends keeping the cyanide ion (CN^-) in drinking water below 1.9 μM (0.2 mg/L) [23, 25–27]. While certain industrial applications exploit cyanide's ability to form less toxic metal complexes, the development of organic-based detection methods offers a safer and potentially more effective approach [28–31]. Rhodamines, known for their dual roles as fluorophores, present a valuable platform for multifunctional sensing. On the other hand, Daphnia magna, often referred to as water fleas, has become invaluable as a live biosensor in environmental monitoring thanks to its remarkable sensitivity to a broad range of chemical pollutants. Their transparent bodies make it straightforward for researchers to observe physiological and behavioral changes [32, 33]. With their rapid reproductive rates, short life spans, and well-documented ecotoxicological characteristics, these organisms are particularly well-suited for evaluating water quality and detecting toxic substances, including heavy metals, pesticides, and emerging contaminants [34]. More recently, live D. magna have been incorporated into advanced sensor systems, enabling real-time, on-site detection of pollutants in aquatic settings and offering an efficient, cost-effective approach to environmental risk assessment [35]. In this study, we report on the synthesis of a novel rhodamine derivative bearing a phenyl group. Following synthesis, we evaluated its ion-detection capabilities using colorimetric analysis of real water samples, drugs, and biological systems, as well as spectroscopic analyses. Moreover, to emphasize the effectiveness of the sensor mechanism, the study has been supplemented with imaging of paper, smartphones, and MCF-7 cells (human breast cancer cell line, ATCC HTB-22). Additionally, *in vivo* tests were performed on live *Daphnia magna* (water fleas) to demonstrate that the system can be studied under in vivo conditions alongside *in vitro* studies.

2. Results and Discussions

2.1 Preparation of a Bis(rhodamine)-Phenyl Hybrid. The potential technical applications of open- and closed-form rhodamine-based compounds encourage their study. In this context, the multistep synthesis of a novel bis-rhodamine-phenyl hybrid, **Rh-Ph-Rh**, was achieved. As documented in the literature, one precursor, Rh-NH_2, was generated by reacting ethylene diamine with rhodamine B (**1**) in ethanol (Scheme S1 and Figure S1) [42]. Then, using an acetic acid catalyst, the Rh-NH_2 reaction with $Ph(CMeO)_2$ in ethanol was carried out overnight at the ethanol boiling point, affording the target probe Rh-Ph-Rh in 78% yield (Scheme 1 and Figure S2). On the other hand, the NMR spectrum of the Rh-Ph-Rh interaction with aluminum ions was obtained, and shifts in the aromatic regions were observed. This suggested that the lactam ring may have opened as a result of the interaction (Figure S3) [28]. Aluminum ions function as Lewis acids and strongly interact with carbonyl oxygen. This interaction causes the ring to open in the presence of aluminum ions, leading to a noticeable color change. NMR spectra also confirm this process (Figure S3). Subsequently, adding $[Bu_4N]CN$ removes the aluminum ions from the system, enabling the amide nitrogen to re-form the lactam ring (Scheme S1). To better understand the binding morphology, we also performed mass spectrometry in conjunction with NMR. Additionally, the mass for the Rh-Ph-Rh-

Al^{3+} complex was detected as 1397,3563 (calculated for $C_{70}H_{78}Al_2Cl_6N_8O_4$: m/z $[M + K]^+$ 1397,3549) (Figure S4B) using high-resolution mass spectrometry (HRMS, ESI-TOF). All this data confirms the synthesis and aluminum-probe interaction.

Scheme 1

2.2 Spectroscopic Response. Following the synthesis of the **Rh-Ph-Rh** probe, its ability to detect various ions was evaluated using UV-Vis and fluorescence spectroscopy. To ensure environmentally friendly conditions, all experiments were initially conducted in water (Fig. 1). The probe was exposed to a range of ions, with a notably strong response observed with aluminum ions, even in tap water samples. Interestingly, after fifteen minutes, the probe also interacted with fluoride ions, producing a weak response (Figure S5A). Overall, time-course studies showed that the interaction between the probe and aluminum ions peaked at about 5 minutes and then stabilized (Figures S5B and S5D). After about fifteen minutes, a slight interaction with fluoride ions became noticeable, though it was clearly weaker than the response observed for aluminum ions. Further examination of timing and solvent conditions led to pH studies, which showed that a neutral environment (around pH 7), both with and without 10 mM HEPES buffer, provided the most favorable conditions for these interactions (Figure S5C and S5D). Even though comparable results were achieved in plain aqueous solutions, buffered pure water was ultimately considered the better choice. This is because aluminum ions tend to form hydroxyl complexes in water, anions can be sensitive to pH changes, and pH fluctuations can directly influence fluorescence intensity [43]. Taking all these factors into account, the optimal setup was determined to be water with HEPES buffer as the solvent. Based on these optimization efforts, the optimal conditions for using the probe were determined: water as the solvent, pH 7 in a HEPES buffer (10 mM), and a five-minute interaction time. The function of probes bearing a rhodamine unit involves ring opening triggered by environmental factors or by interactions with specific ions. This is indicated by the appearance of a characteristic UV-Vis absorption peak around 560 nm, along with a visible color change. UV-Vis studies in water showed a peak at 560 nm, confirming that **Rh-Ph-Rh** undergoes ring opening only in the presence of Al^{3+} ions (Fig. 1A). In addition to UV-Vis spectroscopy, fluorescence spectroscopy was also employed to investigate the interaction of **Rh-Ph-Rh** with various ions. Upon excitation at 500 nm, the probe emitted strongly at 581 nm, particularly in the presence of Al^{3+} in water (Fig. 1B). This intense fluorescence confirms that the probe acts as a selective turn-on sensor for Al^{3+} ions. These fluorescence results are consistent with our UV-Vis data, further proving the probe's selectivity for Al^{3+}. To test the practical potential of **Rh-Ph-Rh**, its selectivity was assessed in the presence of other metal cations. In water, the probe showed excellent selectivity for Al^{3+}, with no interference from other ions. Interestingly, upon addition of cyanide, the fluorescence intensity of the Rh-Ph-Rh–Al^{3+} complex decreased significantly (Fig. 1C). This suggests that the Rh-Ph-Rh–Al^{3+} complex can also serve as an effective turn-off fluorescent sensor for detecting cyanide in water. After completing the general spectral studies, we performed fluorescence titrations to investigate the interaction of the **Rh-Ph-Rh** molecule with aluminum ions (Figure S6). As the concentration of Al^{3+} ions increased, the probe's fluorescence intensity rose steadily and leveled off at 2 μM Al^{3+} (Figure S6A). We determined the limit of detection (LOD) and limit of quantification (LOQ) using

the equations described in the experimental section. The calculated LOD and LOQ were 358 nM and 1.08 μM, respectively (Fig. 1D). These results demonstrate that the **Rh-Ph-Rh** probe can detect Al^{3+} ions in water with high sensitivity, achieving detection limits in the nanomolar to low micromolar range. The reversible interaction between the Rh-Ph-Rh-Al^{3+} complex and cyanide ions indicated that this system could serve as a sensor for CN^- anions (Fig. 1C). To test this, we performed fluorescence titrations across increasing cyanide concentrations, confirming our hypothesis. As the $[Bu_4N]CN$ concentration increased, the fluorescence intensity at 581 nm steadily declined, leveling off at about 3.2 μM (Figure S6B). The calculated LOD and LOQ for cyanide ions were 619 nM and 1.88 μM, respectively (Fig. 1E). These findings demonstrate the complex's high sensitivity and precision for detecting cyanide ions. To see how well **Rh-Ph-Rh** could work as a sensor, we also tested how strongly it binds to Al^{3+} ions using a Job's plot experiment (explained in detail in the experimental section). By tracking fluorescence intensity across mixtures with varying Rh-Ph-Rh-Al^{3+} ratios, we found that they form a 1:2 complex (Figure S7). Next, we used fluorescence titration data to calculate the binding constant (K_a) for Al^{3+}, which was 3.13×10^{11} M^{-2}. This high value indicates a strong affinity of the probe for aluminum ions (Figure S8). Overall, these findings suggest that **Rh-Ph-Rh** could be an effective sensor for detecting Al^{3+} ions.

Figure 1

In the first phase of this study, we investigated probe **Rh-Ph-Rh** as a potential sensor for detecting aluminum and cyanide in water. For this purpose, the performance of the probe **Rh-Ph-Rh** was compared with that of previously reported sensors targeting the same analyses to assess the practical applicability of this sensor candidate. Table 1 shows that our sensor candidate behaves similarly to existing sensors, suggesting its potential to detect cyanide and aluminum in water [28, 30, 43–51]. This sensor candidate offers a few advantages over earlier systems. It's a new bis-rhodamine-substituted organic that enables fast, displacement-based detection of Al^{+3} (within 5–10 minutes) and CN^- (within 5 minutes), both at nanomolar concentrations (Fig. 1). While rhodamine-based sensors for Al^{3+} are fairly common, most struggle to provide a meaningful response to cyanide. Once the probe forms a complex with Al^{3+}, it can be used as a "turn-off" sensor for CN^-, doing so quickly and selectively, even in the presence of other cations and anions (Fig. 1C). In summary, this creates a dual-function sensing platform. Additionally, the sensing process is reversible, allowing reuse for up to five cycles (Figs. 7 and S12), and the detection limits are comparable to or better than those reported in the literature.

Table 1

Comparison of some Al^{3+} and CN^- selective chemosensors.

Reference	Sensor	Sensing ions	LOD
[28]		Al^{3+}	857 nM
		CN^-	680 nM
[30]		Al^{3+}	1.35 μM
		CN^-	0.36 μM
[44]		Al^{3+}	4.32 μM
[45]		Al^{3+}	3.36 μM
[46]		Al^{3+}	392 nM
[47]		Al^{3+}	10.0 μM
[48]		CN^-	0.86 μM
[49]		CN^-	6.67 μM
[50]		CN^-	2.41 μM
[51]		CN^-	4.30 μM
This study		Al^{3+}	358 nM
		CN^-	619 nM

Table 1

2.3 Practical Application and Smartphone-Based RGB Colorimetric Analysis. In addition to spectroscopic techniques, simple tools for determining target analytes without expensive equipment make sensor candidates even more popular for field studies. Therefore, straightforward and effective methods, such as filter paper and colorimetric assays, can complement advanced instruments in evaluating potential sensor candidates. In this context, we began by observing how the probe's color changed in water when exposed to various metal ions. Notably, the probe **Rh-Ph-Rh** exhibited a color change upon exposure to aluminum ions in water, indicating its potential as a visual sensor for aluminum detection. After conducting colorimetric studies in water to develop an easy-to-use detection method for Al^{3+} and CN^-, we prepared test strips by soaking filter paper in probe solutions (Fig. 2). These strips exhibited a quick, visible color change when exposed to solutions containing aluminum, especially under sunlight or UV light. Moreover, test strips pretreated with the Rh-Ph-Rh-Al^{3+} complex rapidly lost their color upon exposure to cyanide, making them useful for detecting cyanide in environmental or

waste samples (Fig. 2). These Rh-Ph-Rh-based test kits offer a simple, affordable, and portable way to detect aluminum and cyanide ions, especially in field environments where advanced lab equipment is unavailable. In conclusion, this straightforward visual method provides an effective means of detecting aluminum and cyanide ions.
Figure 2

Alongside traditional water-based and paper test methods, we have also adopted smartphone-based RGB colorimetric analysis, a technique that has gained significant traction recently, to deepen our understanding of how the probe functions in real-world settings. In this case, real-time RGB analysis using a smartphone was conducted to evaluate the probe's ability to detect Al^{3+} on-site. Test and control solutions were prepared by mixing varying concentrations of Al^{3+} (0–1.6 μmol/L) with probe **Rh-PP-Rh** in water (Figs. 3A, 3B, and S9). Images of all samples were captured under standardized conditions, with a fixed distance of 20 cm between the smartphone camera and the solutions. RGB values were extracted using mobile applications, and the average RGB intensity (R + G + B)/3 was plotted against Al^{3+} concentration (Fig. 3C) [52]. A logarithmic plot revealed a strong linear correlation (R^2 = 0.9446) between RGB intensity and Al^{3+} concentration (Fig. 3D). A control sample containing 5.0 μmol/L Al^{3+} was analyzed to validate the calibration. The corresponding logarithmic RGB intensity value (2.33) closely matched the calculated concentration of 0.48 μmol/L from the calibration curve, consistent with expectations. These findings confirm that the probe functions effectively as a field-deployable sensor for on-site detection of Al^{3+} via smartphone-based RGB analysis.

Figure 3

2.4 Real-World Applications. In addition to exploring practical applications, we tested the probe on various real-water samples, including groundwater, tap water, and drinking water (Figure S10). We also examined surplus aluminum-containing wipes and gel deodorants, which are commonly used to treat or prevent hyperhidrosis. For each sample, we added known amounts of Al^{3+} and then measured the resulting fluorescence using fluorescence spectroscopy. As shown in Table 2, the probe detected Al^{3+} in all matrices, with recoveries ranging from 98.3% to 101.8%, confirming that the probe provides accurate and reliable measurements across samples. Notably, the wipes and gel deodorants contained significant amounts of aluminum. This emphasizes the need for more careful use and raises environmental concerns; once discarded, these materials can leach aluminum into groundwater, contributing to water pollution.

Table 2

Analytical results for the determination of Al^{3+} in real water samples and antiperspirants (wipes and jel deodorants)

Sample	Al^{3+}added ($\mu molL^{-1}$)	Al^{3+}found ($\mu molL^{-1}$)	Recovery (%)
Tap Water	0.0	0.63	0.0
	0.5	1.12	98.9
	1.5	1.66	101.8
	2.0	2.65	101.1
	2.5	3.16	101.2
Ground Water	0.0	0.48	0.0
	0.5	0.98	99.8
	1.5	1.46	98.3
	2.0	2.48	99.8
	2.5	2.95	98.8
Bottled Water	0.0	0.61	0.0
	0.5	1.12	101.6
	1.5	1.64	101.3
	2.0	2.60	99.4
	2.5	3.11	99.6
Wipes	0.0	1.23	0.0
	0.5	1.73	100.1
	1.5	2.22	99.7
	2.0	3.21	99.8
	2.5	3.75	100.6
Jel Deodorant	0.0	1.50	0.0
	0.5	1.96	98.4
	1.5	2.52	100.8
	2.0	3.48	99.4

Sample	Al^{3+}added ($\mu molL^{-1}$)	Al^{3+}found ($\mu molL^{-1}$)	Recovery (%)
	2.5	3.98	99.5

Table 2

2.5 In vitro and In vivo studies. According to the results, the test compound decreased cell viability in a dose-dependent manner, particularly at concentrations of 125–500 µg/mL, where the viability was inhibited by more than 50%, demonstrating its anticancer activity in MCF-7 cells using the WST-1 test, which is advantageous for the newly developed compound. The IC_{50} was calculated to be 31.357 µg/mL (Fig. 4).
Figure 4

To evaluate the practical prospects of the test sample, imaging experiments were performed on human breast cancer cells using negative control, **Rh-Ph-Rh** alone, and Rh-Ph-Rh+Al^{3+}, as shown in Fig. 5. When incubated with the test compound alone, the cells exhibited no fluorescence, indicating that the test material has no fluorescence background. Upon coincubation of the cells with the test compound and subsequent treatment with Al^{3+} (100 µM), pronounced green fluorescence was observed, indicating that the test compound detects Al^{3+} in human breast cells. These results confirmed that the probe **Rh-Ph-Rh** enables effective monitoring of Al^{3+} with high-performance fluorescence imaging.

Figure 5

The fluorescence properties of the probe **Rh-Ph-Rh** in the presence of Al^{3+} in vivo were evaluated using *Daphnia magna*, a standard test organism recommended by USEPA (Figs. 6 and S11). As shown in Fig. 6, neonates in the control group and those exposed to the probe alone showed no detectable fluorescence signal in the green channel. In contrast, neonates incubated with the probe and then exposed to Al^{3+} exhibited a clear green fluorescence signal. These results demonstrate that the probe **Rh-Ph-Rh** can selectively detect Al^{3+} in living organisms.

Figure 6

2.6 Design of Molecular Memory Unit. A major benefit is the capacity of rhodamine-based probe **Rh-Ph-Rh** to reversibly toggle fluorescence in response to Al^{3+} and CN^- ions. Namely, while the interaction of Al^{3+} ions and probe **Rh-Ph-Rh** turns on the fluorescence, subsequent treatment with cyanide turns off the fluorescence. Moreover, demonstrating high reusability, this fluorescence activation-deactivation cycle was repeated up to 12 times. The probe **Rh-Ph-Rh** is thought to form stable complexes with Al^{3+} that are disrupted upon addition of CN^-, leading to a loss of fluorescence (Figs. 7A and S12). Fluorescence "on" and "off" states correspond to logical "1" and "0", respectively, enabling the construction of a molecular logic gate system via this reversible property. In this case, in the absence of

Al^{3+} (Input 1, In_1) or CN^- (Input 2, In_2), the system remains in the "off" state (logic 0). Upon addition of Al^{3+}, the fluorescence turns "on" (logic 1), and subsequent addition of CN^- returns the system to the "off" state (logic 0) (Fig. 7B). The bistable switching of the probe **Rh-Ph-Rh** exhibits non-volatile memory characteristics, maintaining its "on" or "off" state over multiple "write-read-erase-read" cycles (Fig. 7, inset scheme). This optical memory capability enables reliable molecular-level logic operations, offering promising potential for future molecular microprocessors and memory components in integrated logic systems.
Figure 7

Given its practical applications, the work also emphasizes real-world usefulness. The sensor functions colorimetrically, integrates with smartphone-based analysis, and uses simple test strips for quick, low-cost detection. Its effectiveness has been demonstrated not only in real water samples and cosmetic products but also in biological contexts, including cell imaging and both in vitro and in vivo studies with Daphnia magna. Overall, the combination of sensitivity, selectivity, reversibility, and flexibility across different platforms gives this sensor a broader and more practical advantage over many existing systems.

3. Conclusions

In conclusion, the newly synthesized bis-rhodamine-substituted phenyl hybrid probe, **Rh-Ph-Rh**, yielded intriguing results, highlighting its multifunctional capabilities across sensing, imaging, and biomedical applications. **Recognition Capabilities**: **Rh-Ph-Rh** exhibited selective recognition of Al^{3+} ions in aqueous media, with a detection limit of 358 nM. Additionally, in the presence of Al^{3+}, the probe acted as a "turn-off" sensor for cyanide ions, with a detection limit of 619 nM. These dual-mode sensing properties reflect the probe's high sensitivity and selectivity. **Practical Application**: The colorimetric responses on filter paper and the visible color changes upon addition of Al^{3+} demonstrated the probe's suitability for field applications, particularly in environmental monitoring for aluminum and cyanide contamination. **Smartphone-Based RGB Colorimetric Studies**: RGB analysis facilitated smartphone-assisted, *in situ* detection of Al^{3+}, confirming the probe's practicality as a portable, field-deployable sensor. **Real-World Applications**: Recognition experiments have been expanded to include samples from tap water, drinking water, and groundwater, as well as pharmaceuticals, demonstrating the versatility and reliability of **Rh-Ph-Rh** across complex matrices. **Cell Viability and Imaging Studies**: The probe exhibited high cytotoxicity and potent anticancer activity in MCF-7 cells, with an IC_{50} of 31.357 μg/mL. Fluorescence imaging studies confirmed the detection of Al^{3+} within live cells, supporting its use in intracellular sensing. **In Vivo Studies**: Experiments with *Daphnia magna* validated the probe's *in vivo* selectivity for Al^{3+}, with a distinct green fluorescence observed only in Al^{3+}-treated organisms, demonstrating its biosensing capability in living systems. **Molecular Logic Properties**: The reversible ring-opening/closing behavior of **Rh-Ph-Rh** enabled its use as a molecular memory unit.

4. Experimental

4.2. Synthesis of probe (Rh-Ph-Rh)

To a solution of rhodamine B ethylenediamine (Rh-NH_2, 100 mg, 2 equiv.) in ethanol (10 mL), either 1,1'-(1,4-phenylene)bis(ethan-1-one) (Ph$(CMeO)_2$, 17 mg, 1 equiv.) was added. The reaction mixture was stirred under reflux in ethanol. Upon completion of the reaction, the solvent was removed under reduced pressure by TLC. The crude product was purified by recrystallization to yield the desired probe as a pale-yellow solid (88 mg, 78% yield). ^{1}H NMR (400 MHz, DMSO-d6) δ 7.81-7.79 (m, 3H, =CH), 7.61 (m, 3H, =CH), 7.51 (m, 4H, =CH), 7.05 (m, 2H, =CH), 6.32 (m, 12H, =CH), 3.35-3.10 (m, 30H, CH_2, CH_3), 1.88 (s, 6H, CH_2), 1.05 (m, 18H, CH_2, CH_3); ^{13}C NMR (100 MHz, DMSO-d6) δ 167.3, 165.2, 153.8, 153.1, 148.8, 141.2, 131.1, 128.9, 128.4, 127.2, 126.6, 124.1, 122.8, 108.6, 105.5, 97.7, 64.5, 49.9, 44.2, 41.2, 15.2, 12.8 (Figure S2); HRMS (ESI-TOF) m/z: $[M]^+$ calcd for $C_{70}H_{78}N_8O_4$, 1094.6141; found, 1094.6166 (Figure S4A).

4.3. Methodology for Recognition Evaluation

The probe's recognition behavior toward various analytes was systematically evaluated using experimental procedures reported in the literature.[28] To this end, UV–Vis absorption and fluorescence studies were initially conducted to examine the probe's interaction with various ions, while titration experiments with Al^{3+} and CN^- were carried out under controlled conditions to observe spectral changes. The binding stoichiometry was determined using Job's method, and the detection limit (LOD) was calculated from fluorescence titration data using standard analytical approaches. Additionally, the association constant (K_a) was calculated using the Benesi–Hildebrand method. The effect of pH on sensing performance was studied across a wide pH range, and the probe's reversible switching behavior in the presence of Al^{3+} and CN^- ions was evaluated through repeated cycling tests. Furthermore, colorimetric test strips were prepared to assess practical use, and real-sample testing was performed on different water sources to verify the probe's effectiveness under real-world conditions. Detailed experimental procedures are included in the Supplementary Information.

4.3. Biological measurement

The study of cytotoxicity, anticancer activity, and live-cell imaging of the tested compound was conducted using established protocols from the literature [47-49]. MCF-7 human breast cancer cells were cultured under standard conditions, and *in vitro* cytotoxicity was measured with the WST-1 assay to evaluate dose-dependent effects on cell viability. Cellular morphology was observed simultaneously through microscopy to support viability results. Based on the cytotoxicity findings, non-toxic concentrations were selected for live-cell imaging studies, in which the probe's intracellular fluorescence response to aluminum ions was analyzed using confocal microscopy. Furthermore, *in vivo* imaging studies were performed using Daphnia magna as a model organism, following OECD guideline-based procedures [33, 50, 51], to assess the probe's fluorescence behavior in a whole-organism system. Detailed experimental procedures are available in the Supplementary Information.

Declarations

Author Contribution

K. Yararli: Investigation, A.S. Hussein: Investigation, F. Keteci: Investigation, B. Bakan: Writing & editing, O Türbedaroglu: Investigation, T. Sisman: Writing & editing, O. Aksakal: Writing & editing, S. Bayindir: Writing & editing, supervisor, and F. Lafzi: Writing & editing, supervisor.

Acknowledgement

The authors thank the Scientific Research Projects Coordination Unit of Ataturk University (Project No. FCD-2025-15418), Bingol University and Salahaddin University-Erbil for their financial support.

References

1. Sahu, P., Chaturwedi, A. K., Patel, D., Bai, S., Kashyap, N. K., Hait, M., & Patra, G. K. (2025). Rhodamine based chemosensors for metal ions detection: an overview. *Journal of Fluorescence*, 35, 9231–9250.
2. Chen, X., & Wang, Q. (2026). Recent Advances of Optical Sensing Arrays (2019–2025): From Design of Optical Elements to Multidimensional Analysis for Applications. *Analytical Chemistry*, 98, 4, 2633–2679.
3. Picci, G., Montis, R., Gilchrist, A. M., Gale, P. A., & Caltagirone, C. (2024). Fluorescent and colorimetric sensors for anions: Highlights from 2020 to 2022. *Coordination Chemistry Reviews*, *501*, 215561.
4. Sahu, P., Patel, A. R., Pandey, A., & Verma, V. (2025). Fluorescent Rhodamine Sensors for Mercury, Iron, and Copper Ion Detection in Water: Mechanisms and Applications. *Journal of Fluorescence*, 35, 10167–10188.
5. Sultana, T., Mahato, M., Tohora, N., Das, A., Datta, P., & Das, S. K. (2023). Phthalimide-Based Off-On-Off Fluorosensor for Cascade Detection of Cyanide Ions and Picric Acid. *ChemistrySelect*, *8*(13), e202204388.
6. Wang, Y., Wang, X., Ma, W., Lu, R., Zhou, W., & Gao, H. (2022). Recent developments in rhodamine-based chemosensors: A review of the years 2018–2022. *Chemosensors*, *10*(10), 399.
7. Yadav, L., Yadav, P., Laddha, H., Sharma, M., Sharma, P., Agarwal, M., & Gupta, R. (2024). Smartphone based CN–ion sensing in electroplating wastewater and food samples in a simple, economical and rapid manner. *Inorganic Chemistry Communications*, *161*, 112083.
8. Gul, Z., Salman, M., Khan, S., Shehzad, A., Ullah, H., Irshad, M., ... & Altaf, A. A. (2024). Single organic ligands act as a bifunctional sensor for subsequent detection of metal and cyanide ions, a statistical approach toward coordination and sensitivity. *Critical Reviews in Analytical Chemistry*, *54*(7), 2500-2516.

9. Bala, M., Gaddam, M., & Sharma, A. (2025). Perylene-Based Fluorescent and Colorimetric Probes for Multimode Sensing Applications. In *Small Organic Molecules-Based Fluorescent Biosensors and their Applications*, CRC Press. 2025. p. 72-84.
10. El-Shishtawy, R. M., Hussein, M. A., Salam, M. A., Obaid, A. Y., El-Sedik, M., Mohamed, M. B. I., & Aysha, T. (2026). Multi-targeting fluorescence probe based on coumarin receptors for recognition of cyanide and picric acid. *Microchemical Journal*, 222, 117017.
11. Prajapati, S., Hindore, S., & Jana, S. (2025). Selective optical detection and fluorescence sensing of cyanide ion in aqueous medium using rhodamine B based sensor. *Journal of the Indian Chemical Society*, 102 (11), 102141.
12. Zhang, R., Yan, F., Huang, Y., Kong, D., Ye, Q., Xu, J., & Chen, L. (2016). Rhodamine-based ratiometric fluorescent probes based on excitation energy transfer mechanisms: construction and applications in ratiometric sensing. *Rsc Advances*, *6*(56), 50732-50760.
13. Takkar, P., Negi, S., Kakkar, R., & Kumar, R. (2025). Rhodamine based turn-on dual mode chemosensor for the selective recognition of nickel ions: practical and theoretical applications. *RSC advances*, *15*(3), 1641-1657.
14. Sarkar, S., Chatterjee, A., & Biswas, K. (2024). A recent update on rhodamine dye based sensor molecules: a review. *Critical Reviews in Analytical Chemistry*, *54*(7), 2351-2377.
15. Adak, A. K., Shit, M., Sinha, C., & Dutta, B. (2025). Reversible Sensing Execution of a Rhodamine-Based Dyad for the Recognition of Aluminium Ions (Al^{3+}) and Bifluoride Ions (HF^{2-}) and Inhibit Logic Gate. *ES Chemistry and Sustainability*, *5*, 1925.
16. Meng, X., Zhang, Y., Guo, D., & Li, J. (2025). A Ratio Fluorescent Sensor Based on Coumarin and Rhodamine for Sequential Detection of Aluminium Ion and Pyrophosphate and Its Applicability in Arabidopsis Thaliana. *ChemistrySelect*, *10*(4), e202405523.
17. Esquivel, P.V., Ruiz-García, A., Genesco, J., & Montoya, R. (2023). Easy and low-cost transient detection of Al (III) evolution during the galvanic corrosion of aluminum alloys. *Journal of Solid State Electrochemistry*, *27*(11), 3041-3048.
18. Yasar, O. G., Elmas, S. N. K., Aydin, D., & Arslan, F. N. (2024). Al^{3+} selective ratiometric fluorescent and colorimetric chemoprobe and its practical applications in foods, test kits and Smartphone. *Journal of Photochemistry and Photobiology A: Chemistry*, *447*, 115238.
19. Parambil, A. R. U., Kavyashree, P., Silswal, A., & Koner, A. L. (2022). Water-soluble optical sensors: keys to detect aluminium in biological environment. *RSC advances*, *12*(22), 13950-13970.
20. Walton, J. R. (2006). Aluminum in hippocampal neurons from humans with Alzheimer's disease. *Neurotoxicology*, *27*(3), 385-394.
21. Kumari, N., Singh, S., Baral, M., & Kanungo, B. K. (2023). Schiff bases: a versatile fluorescence probe in sensing cations. *Journal of Fluorescence*, *33*(3), 859-893.
22. Mohanty, P., Behura, R., Bhardwaj, V., Dash, P. P., Sahoo, S. K., & Jali, B. R. (2022). Recent advancement on chromo-fluorogenic sensing of aluminum (III) with Schiff bases. *Trends in Environmental Analytical Chemistry*, *34*, e00166.

23. World Health Organization. *Guidelines for Drinking-water Quality*, 4th ed.; WHO: Geneva, **2011**; p 340.
24. Naskar B, Modak R, Sikdar Y et al (2017) Fluorescent sensing of Al^{3+} by benzophenone-based Schiff base chemosensor and live cell imaging applications: Impact of keto-enol tautomerism. *Sens Actuators B Chem* 239:1194–1204.
25. World Health Organization. (2002). *Guidelines for drinking-water quality*. World Health Organization.
26. Singh, M., Nadendla, S., & Kanaparthi, R. K. (2025). A highly sensitive colorimetric and fluorometric sensor for the detection of cyanide. *Journal of Photochemistry and Photobiology A: Chemistry*, *458*, 115957.
27. US Environmental Protection Agency. (1979). Guidelines establishing test procedures for the analysis of pollutants. *Fed. Reg.*, *44*, 69464-69575.
28. Ardahanlı, R., Hussein, A. S., Lafzi, F., Bayindir, S., & Kilic, H. (2025). Water-Driven Cascade Specific Detection of Al (III)/Hg (II) and CN^-/GSH in Real Water Samples. *ACS omega*, *10*(28), 31022-31032
29. Jangir, J., Ranolia, A., Chahal, S., Singh, S., Duhan, A., Dhaka, R. K., ... & Sindhu, J. (2025). Colorimetric reversibility: Aqueous phase recognition of cyanide using smart phone-based devices with real sample analysis. *Microchemical Journal*, *208*, 112259.
30. Bayindir, S., & Hussein, A. S. (2024). Off-On–Off Cascade Recognition of Cyanide, Mercury, and Aluminum Using N/5-Monosubstituted Rhodanines. *ACS omega*, *9*(15), 17602-17615.
31. Hussein, A. S., Bayindir, S., & Toprak, M. (2026). Buffer-Selective Rhodamine-Based Fluorescent Sensor for Selective Cascade Detection of Aluminum, Mercury and Cyanide. *ChemistrySelect*, *11*(5), e06947.
32. Lotfi, S., Ahmadi, S., Azimi, A., & Kumar, P. (2025). In silico aquatic toxicity prediction of chemicals toward Daphnia magna and fathead minnow using Monte Carlo approaches. *Toxicology Mechanisms and Methods*, *35*(3), 305-317.
33. OECD. (2004). *Test No. 202: Daphnia sp. Acute Immobilisation Test*. OECD Publishing.
34. Tkaczyk, A., Bownik, A., Dudka, J., Kowal, K., & Ślaska, B. (2021). Daphnia magna model in the toxicity assessment of pharmaceuticals: A review. *Science of The Total Environment, 763*, 143038.
35. Jeong, T. Y., & Simpson, M. J. (2019). Daphnia magna metabolic profiling as a promising water quality parameter for the biological early warning system. *Water research*, *166*, 115033.
36. Hussein, A. S., Lafzi, F., Bayindir, S., Kilic, H., & Toprak, M. (2024). A Novel Rhodamine-Phenolphthalein Architecture for Selective Mercury Ion Detection in Aqueous Media. *ChemPlusChem*, *89*(5), e202300649.
37. Giacobello, F., Mollica-Nardo, V., Foti, C., Ponterio, R. C., Saija, F., Trusso, S., Sponer, J., Cassone, G., & Giuffrè, O. (2022). Hydrolysis of Al3+ in Aqueous Solutions: Experiments and Ab Initio Simulations. Liquids, 2(1), 26-38.
38. Kundu, B. K., Mandal, P., Mukhopadhyay, B. G., Tiwari, R., Nayak, D., Ganguly, R., & Mukhopadhyay, S. (2019). Substituent dependent sensing behavior of Schiff base chemosensors in detecting Zn^{2+} and

Al^{3+} ions: Drug sample analysis and living cell imaging. *Sensors and Actuators B: Chemical*, *282*, 347-358.

39. Das, D. K., Kumar, J., Bhowmick, A., Bhattacharyya, P. K., & Banu, S. (2017). 2-Hydroxyacetophenone and ethylenediamine condensed Schiff base: Fluorescent sensor for Al3+ and PO43−, biological cell imaging and INHIBIT logic gate. *Inorganica Chimica Acta*, *462*, 167-173.
40. Li, Y., Liao, C., Huang, S., Xu, H., Zheng, B., Du, J., & Xiao, D. (2016). A selective fluorescent probe based on bis-Schiff base for “turn-on” detection of Al^{3+} and cysteine by different mechanisms. *RSC Advances*, *6*(30), 25420-25426.
41. Selvan, G. T., Kumaresan, M., Sivaraj, R., Enoch, I. V., & Selvakumar, P. M. (2016). Isomeric 4-aminoantipyrine derivatives as fluorescent chemosensors of Al^{3+} ions and their molecular logic behaviour. *Sensors and Actuators B: Chemical*, *229*, 181-189.
42. Oguz, M., Gul, A., Kursunlu, A. N., & Yilmaz, M. (2021). A bifunctional and multi-responsive fluorescent sensor for toxic analytes in the aqueous medium: Easy synthesis, NIR-visible effect, imaging in living cells. *Journal of Molecular Liquids*, *336*, 116861.
43. Wang, T., Shen, L., Wang, H., & Zhang, N. (2021). A highly selective fluorescent sensor for ratiometric detection of cyanide in aqueous solution and solid states. *Journal of Molecular Structure*, *1231*, 129671.
44. Kang, J., Huo, F., Zhang, Y., Chao, J., Glass, T. E., & Yin, C. (2019). A novel near-infrared ratiometric fluorescent probe for cyanide and its bioimaging applications. *Spectrochimica Acta Part A: Molecular and Biomolecular Spectroscopy*, *209*, 95-99.
45. Li, Y., Yao, C., Zhong, D., Li, H., Liu, B., Feng, Z., ... & Yang, Z. (2020). Phosphorescent cyanide sensor based on a 2-phenylpyridine (ppy)-type cyclometalated Ir(III) complex bearing dimesitylboron group with concentration distinguishing ability. *Journal of Organometallic Chemistry*, *917*, 121274.
46. Li, L., Li, X., Wang, X., Zhang, Q., Zheng, C., Jing, Y., & Xie, H. (2025). Enhanced near-infrared Ru (II) complex fluorescence sensor for sensitive sensing of Al^{3+} and cell imaging. *Spectrochimica Acta Part A: Molecular and Biomolecular Spectroscopy*, *339*, 126294.
47. Bakan, B., Gülcemal, S., Akgöl, S., Hoet, P. H., & Yavaşoğlu, N. Ü. K. (2020). Synthesis, characterization and toxicity assessment of a new polymeric nanoparticle, l-glutamic acid-gp (HEMA). *Chemico-Biological Interactions*, *315*, 108870.
48. Xu, J., Pan, J., Jiang, X., Qin, C., Zeng, L., Zhang, H., & Zhang, J. F. (2016). A mitochondria-targeted ratiometric fluorescent probe for rapid, sensitive and specific detection of biological SO_2 derivatives in living cells. *Biosensors and Bioelectronics*, *77*, 725-732.
49. Ping, Y., Liu, M., Yu, Y. *et al.* A Long-wavelength Colorimetric and Fluorescent Chemodosimeter for Monitoring Cu^{2+} in the Environment and Living Systems. *J Fluoresc* **35**, 10551–10560 (2025).
50. OECD. (2012). Test No. 211: Daphnia magna reproduction test, OECD guidelines for the testing of chemicals, section 2.

51. Aksakal, O., Dane, H., Gur, C., & Sisman, T. (2025). Chronic toxicity of tetraconazole and penconazole to Daphnia magna: Insights of growth, reproduction and gene expression changes. *Science of The Total Environment*, *967*, 178774.

Schemes

Scheme 1 is available in the Supplementary Files section

Figures

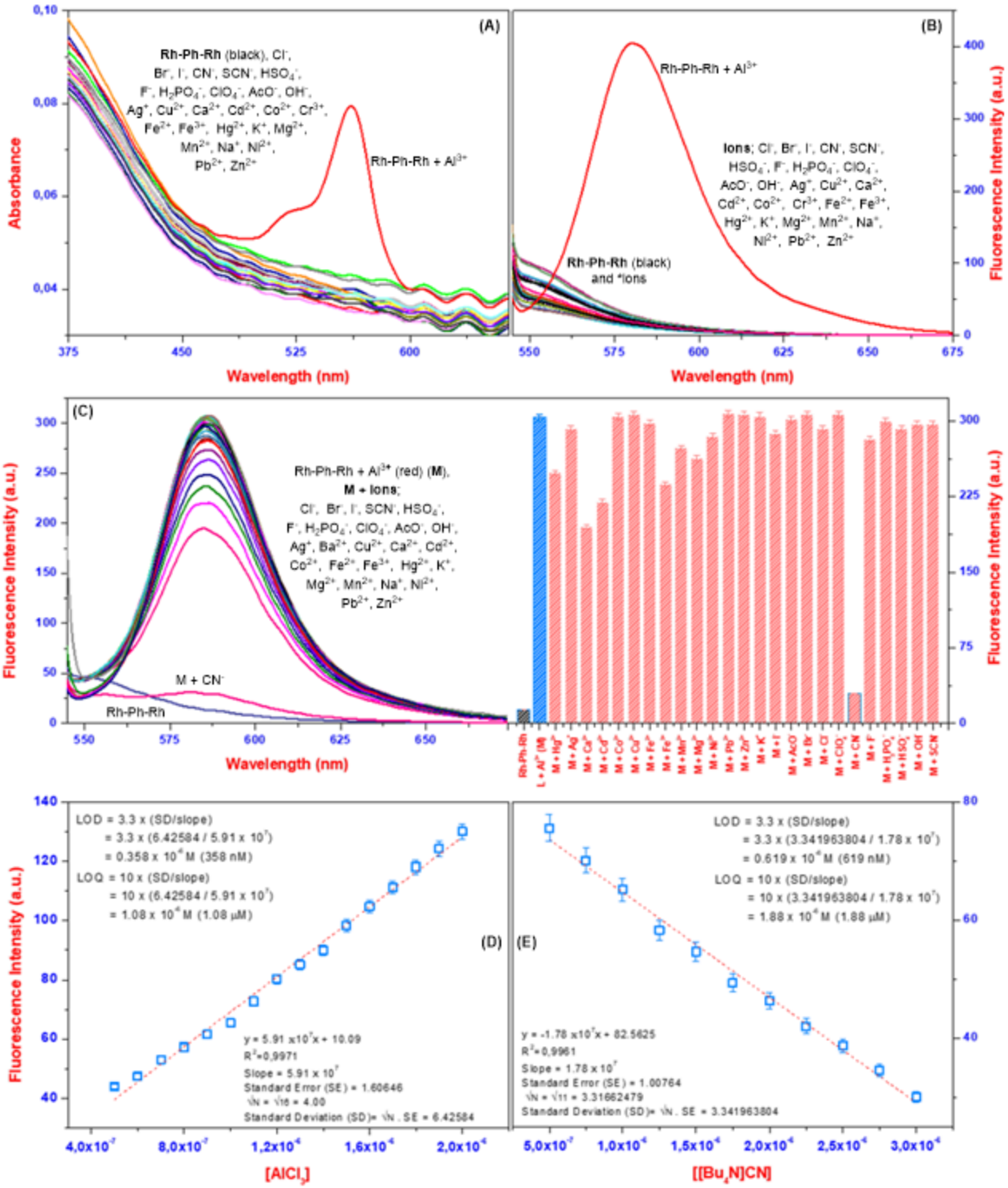


Figure 1

The UV-Vis (**A**) and fluorescence (**B**) spectras of Rh-Ph-Rh with the absence and presence of ions, (**C**) the fluorescence spectra and bar graphics of Rh-Ph-Rh upon adding different ions up to 1 equivalent in water, and the changes in fluorescence intensity of Rh-Ph-Rh and Rh-Ph-Rh-Al^{3+} with the increasing concentration of $AlCl_3$ (**D**), and $[Bu_4N]CN$ (**E**).

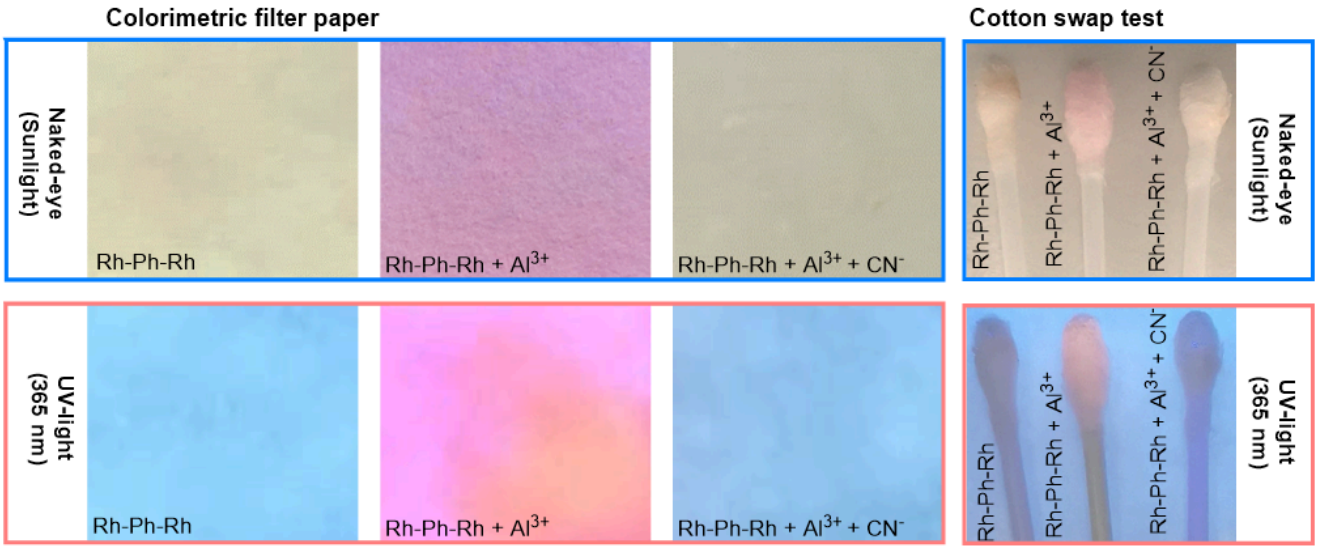


Figure 2

The sunlight and UV light at 365 nm cause color changes in photographs depicting the formation of Rh Ph-Rh and Rh-Ph-Rh-Al^{3+} with $AlCl_3$ and $[Bu_4N]CN$ as observed with filter paper, and colorimetric cotton swabs

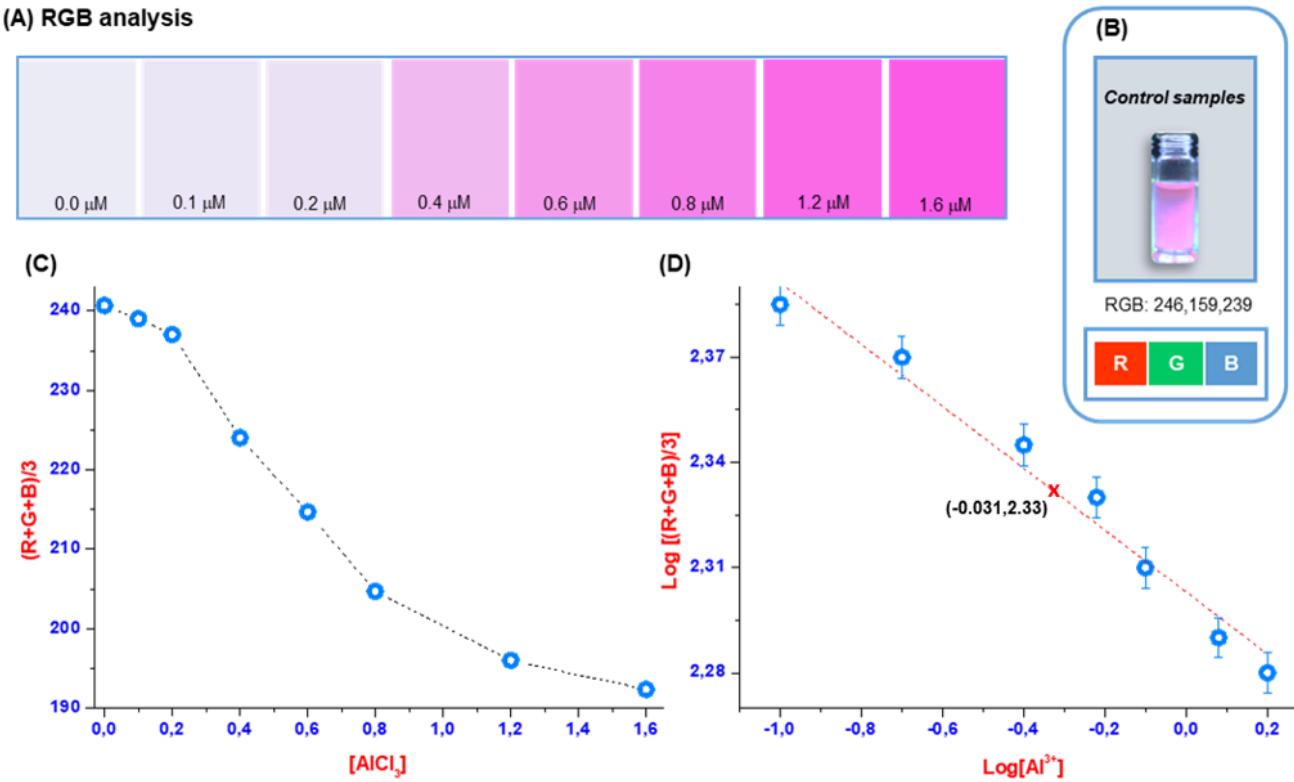


Figure 3

(**A**) Color changes of Rh-Ph-Rh with varying Al^{3+} concentrations; (**B**) Workflow for Al^{3+} quantification in control samples using RGB analysis; (**C**) Calibration curve for Al^{3+} concentrations from 0–1.6 µmol/L; (**D**) Calibration curve presented on a logarithmic scale.

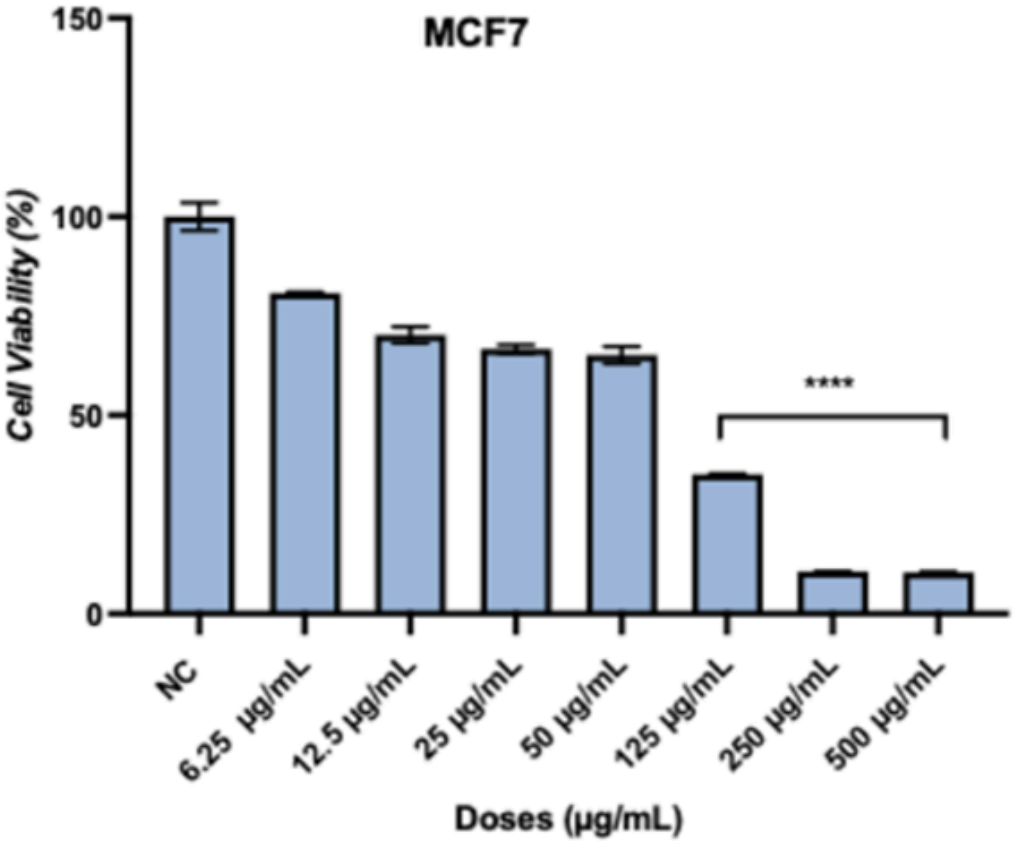


Figure 4

Cytotoxicity test results after 24 h exposure at different test sample concentrations in the MCF-7 cell line by WST-1 assay. All data obtained from three independent replicates and presented as mean± SD.

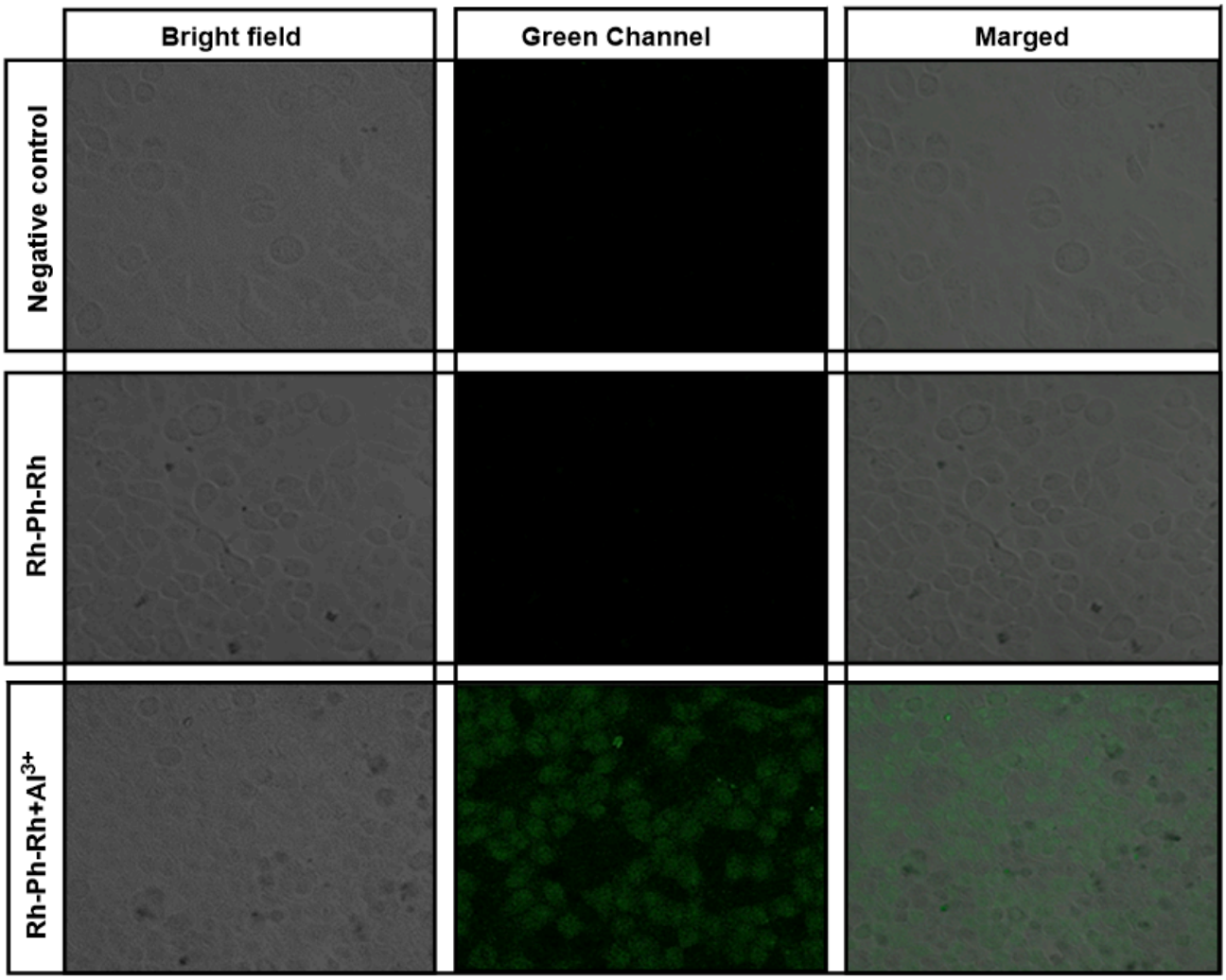


Figure 5

Confocal fluorescence microscopic images in MCF-7 cells incubated with 50 μg/mL of Rh-Ph-Rh for 30 min, followed by an additional 30 min. incubation with Al^{3+} at 100 μM concentration. (λex = 543 nm. λem = 600–700 nm).

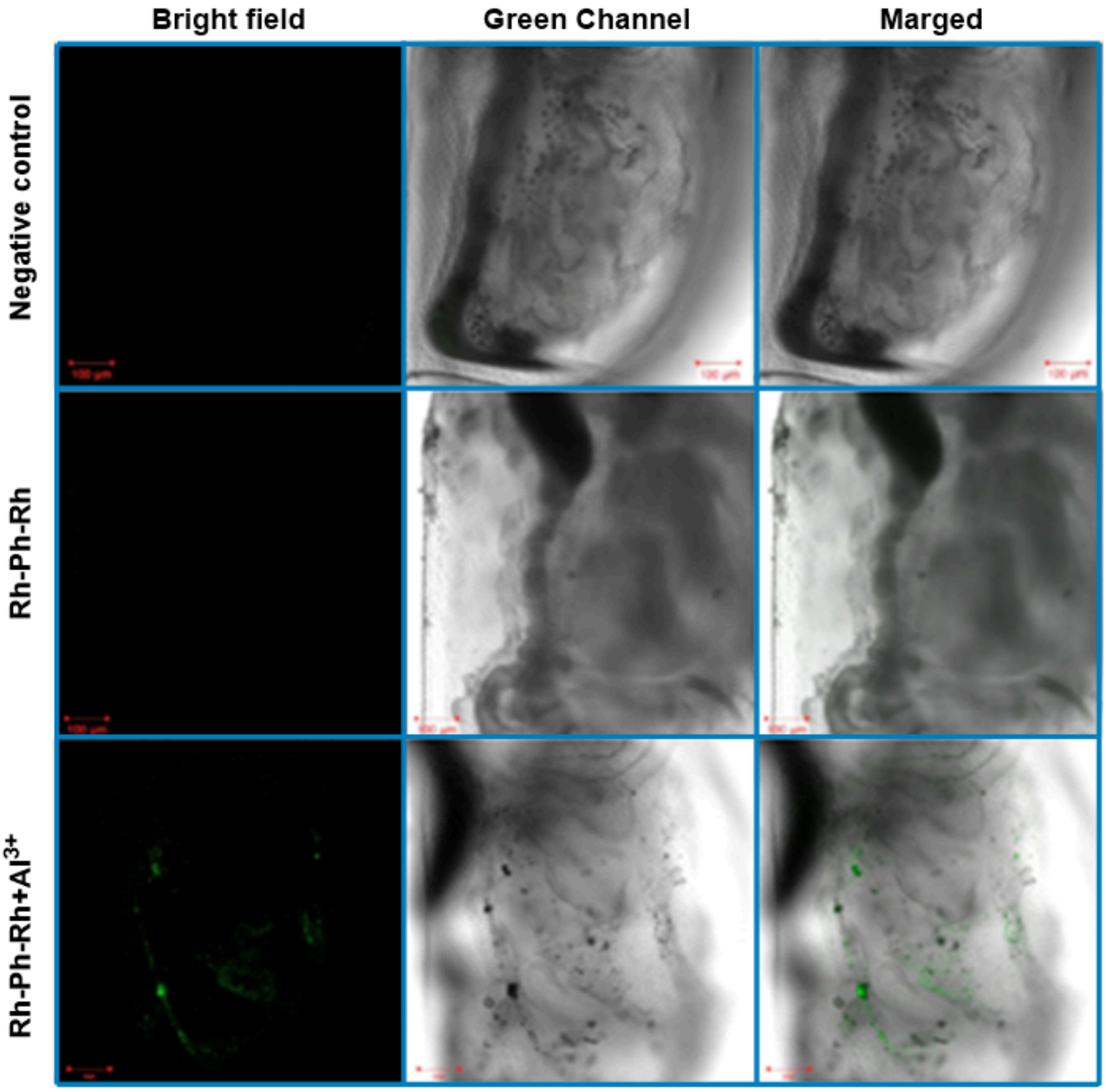


Figure 6

Fluorescence images of *Daphnia magna*: control group, incubated with 50 µg/mL of the Rh-Ph-Rh only, and incubated with 50 µg/mL of the probe followed by 100 µM Al^{3+} (*Scale bar for neonates = 200 µm; scale bars for magnified images = 100 µm*).

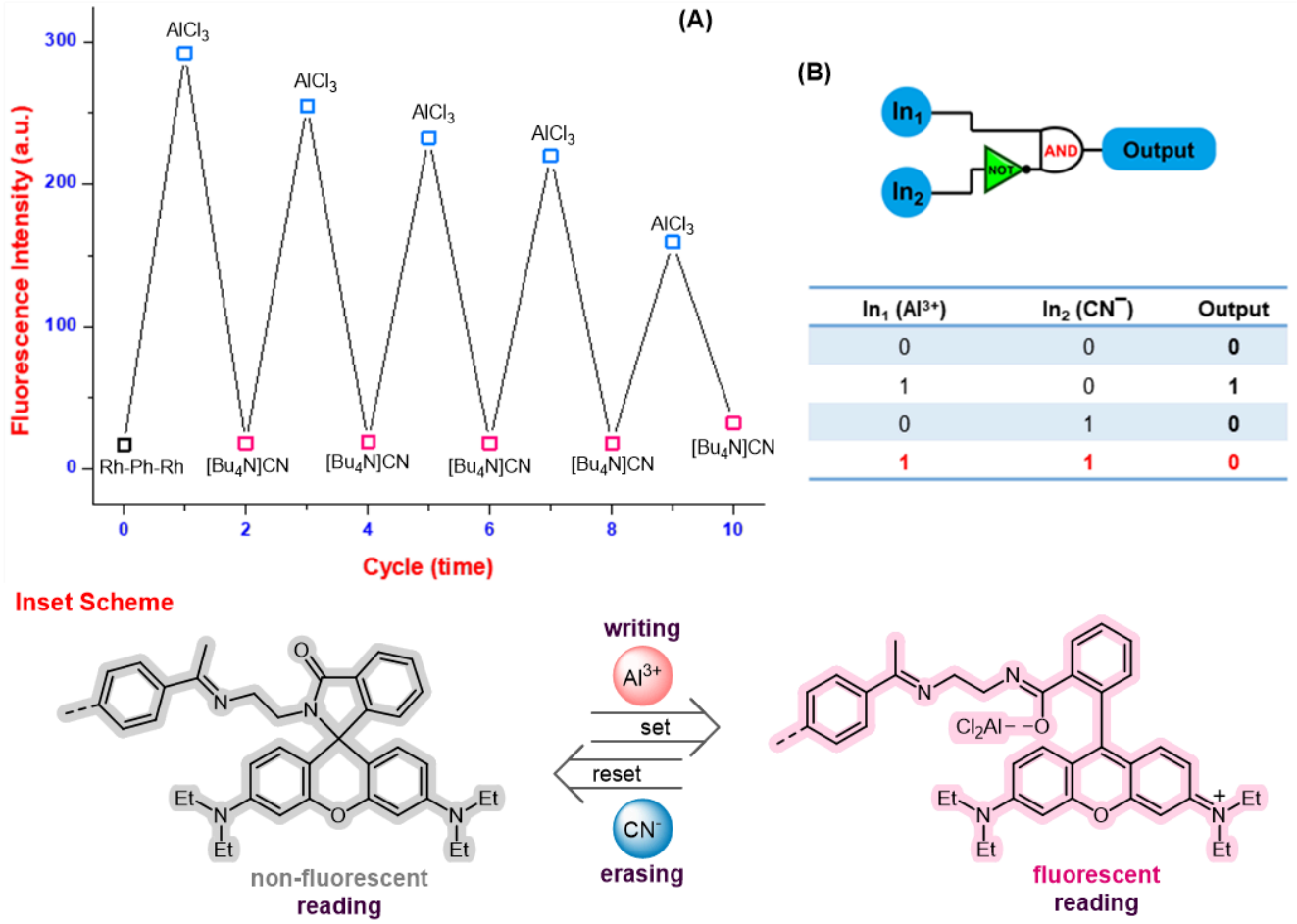


Figure 7

The reversible switching of the fluorescence intensity of Rh-Ph-Rh-Al^{3+}/$[Bu_4N]CN$ (**A**), and (**B**) the "IMPLICATION" logic gate. **Inset scheme:** Reversible logic processes with *"reading-writing-reading-erasing-reading"* activities are revealed by the feedback loop.

Supplementary Files

This is a list of supplementary files associated with this preprint. Click to download.

- SupplementaryData.docx
- GraphicalAbstract.docx
- Scheme1.docx